


# Geometries and electronic structures of $Zr_nCu$ ($n$ = 2-12) clusters: A joint machine-learning potential density functional theory investigation

Yizhi Wang(王一志), Xiuhua Cui(崔秀花), Jing Liu(刘静), Qun Jing(井群), Haiming Duan(段海明), and Haibin Cao(曹海宾)

**Citation:**Chin. Phys. B, 2024, 33 (**1**): 016109. DOI: 10.1088/1674-1056/acd5c2
Journal homepage: http://cpb.iphy.ac.cn; http://iopscience.iop.org/cpb

**What follows is a list of articles you may be interested in**

---

## Hydrogen evolution reaction between small-sized $Zr_n$ ($n$ = 2–5) clusters and water based on density functional theory

Lei-Lei Tang(唐雷雷), Shun-Ping Shi(史顺平), Yong Song(宋永), Jia-Bao Hu(胡家宝), Kai Diao(刁凯), Jing Jiang(蒋静), Zhan-Jiang Duan(段湛江), and De-Liang Chen(陈德良)
Chin. Phys. B, 2023, 32 (**6**): 066106. DOI: 10.1088/1674-1056/aca7ec

## Probing the effects of lithium doping on structures, properties, and stabilities of magnesium cluster anions

Xiao-Yi Zhang(张小义), Ya-Ru Zhao(赵亚儒), Hong-Xing Li(李红星), Kai-Ge Cheng(成凯格), Zi-Rui Liu(刘子锐), Zhi-Ping Liu(刘芷萍), and Hang He(何航)
Chin. Phys. B, 2023, 32 (**6**): 066102. DOI: 10.1088/1674-1056/acc51f

## Probing structural and electronic properties of divalent metal $Mg_{n+1}$ and $SrMg_n$ ($n$ = 2–12) clusters and their anions

Song-Guo Xi(奚松国), Qing-Yang Li(李青阳), Yan-Fei Hu(胡燕飞), Yu-Quan Yuan(袁玉全), Ya-Ru Zhao(赵亚儒), Jun-Jie Yuan(袁俊杰), Meng-Chun Li(李孟春), and Yu-Jie Yang(杨雨杰)
Chin. Phys. B, 2022, 31 (**1**): 016106. DOI: 10.1088/1674-1056/ac04aa

## Growth of PbS nanoclusters on specific sites of programmed oligodeoxynucleotides

Lu Ying (陆颖), Teng Cui-Juan (滕翠娟), Li Ying (李颖), Wang Hui (王惠), Xu Chun-Hua (徐春华), Hu Shu-Xin (胡书新), Li Ming (李明)
Chin. Phys. B, 2015, 24 (**1**): 016101. DOI: 10.1088/1674-1056/24/1/016101

## Silicon micro-hemispheres with periodic nanoscale rings produced by the laser ablation of single crystalline silicon

Chen Ming (陈明), Li Shuang (李爽), Cui Qing-Qiang (崔清强), Liu Xiang-Dong (刘向东)
Chin. Phys. B, 2013, 22 (**10**): 106101. DOI: 10.1088/1674-1056/22/10/106101

---

# Geometries and electronic structures of $Zr_nCu$ ($n = 2$–12) clusters: A joint machine-learning potential density functional theory investigation

Yizhi Wang(王一志)[1,2], Xiuhua Cui(崔秀花)[1,2,†], Jing Liu(刘静)[1,2], Qun Jing(井群)[1,2], Haiming Duan(段海明)[1,2,‡], and Haibin Cao(曹海宾)[3]

[1] *Xinjiang Key Laboratory of Solid State Physics and Devices, Xinjiang University, Urumqi* 830017, *China*
[2] *School of Physical Science and Technology, Xinjiang University, Urumqi* 830017, *China*
[3] *Department of Physics, College of Sciences, Shihezi University, Shihezi* 832000, *China*

(Received 11 January 2023; revised manuscript received 4 May 2023; accepted manuscript online 16 May 2023)

Zr-based amorphous alloys have attracted extensive attention because of their large glassy formation ability, wide supercooled liquid region, high elasticity, and unique mechanical strength induced by their icosahedral local structures. To determine the microstructures of Zr–Cu clusters, the stable and metastable geometry of $Zr_nCu$ ($n = 2$–12) clusters are screened out via the CALYPSO method using machine-learning potentials, and then the electronic structures are investigated using density functional theory. The results show that the $Zr_nCu$ ($n \geq 3$) clusters possess three-dimensional geometries, $Zr_nCu$ ($n \geq 9$) possess cage-like geometries, and the $Zr_{12}Cu$ cluster has icosahedral geometry. The binding energy per atom gradually gets enlarged with the increase in the size of the clusters, and $Zr_nCu$ ($n = 5$, 7, 9, 12) have relatively better stability than their neighbors. The magnetic moment of most $Zr_nCu$ clusters is just $1\mu_B$, and the main components of the highest occupied molecular orbitals (HOMOs) in the $Zr_{12}Cu$ cluster come from the Zr-d state. There are hardly any localized two-center bonds, and there are about 20 $\sigma$-type delocalized three-center bonds.

**Keywords:** geometries and electronic structures, magnetic and chemical bonds, machine learning potentials, Zr–Cu clusters

**PACS:** 61.46.Bc, 31.15.ej, 36.40.–c, 36.40.Cg **DOI:** 10.1088/1674-1056/acd5c2

## 1. Introduction

Amorphous alloys, also called metallic glasses (MGs), have unique physical properties[1–7] due to their short-range ordered but long-range disordered atomic structures[8] obtained from the crystallization process with an extremely high cooling rate.[9] Since the first discovery of bulk Zr–Al–Ni–Cu compound,[10] Zr-base amorphous alloys have attracted widespread attention due to their high glassy formation ability, wide supercooled liquid region, excellent mechanical properties[4,11–13] compared with Fe-base,[1] Mg-base,[3] Co-base[14] and Ni-base[15,16] amorphous alloys.

Previous studies show that the microstructures especially the icosahedral clusters play an important role in the formation and the physical properties of amorphous alloys;[4,17–25] hence, intensive efforts have been made to investigate the stable geometries, electronic structures, and physical properties of Zr-base clusters and amorphous alloys.[26–30] Jiang *et al.*[26] studied the geometry of $Cu_nZr_{13-n}$ ($n = 3$–10) clusters using density functional theory (DFT) and they found $Zr_7Cu_6$ is more stable than others. Wang *et al.*[29] studied the $Cu_6Zr_7$ and $Cu_8Zr_5$ clusters and found that the stability of these icosahedral clusters has a relation to the glassy formation ability (GFA). Sha *et al.*[30] established a direct connection between the electronic structure of the basic clusters in MGs and the glass-forming ability of MGs, providing a new avenue to examine the GFA of MGs. Based on the molecular dynamics simulation results of the $Cu_{60}Zr_{40}$ model MG, Lekka *et al.*[31] selected two representative clusters ($Cu_7Zr_6$ and $Cu_{10}Zr_5$) in the $Cu_{60}Zr_{40}$ model, and calculated their interconnections as touching or interpenetrating using DFT. Yang *et al.*[32] obtained basic polyhedral clusters of near-eutectic composition by considering the dense packing and random arrangement of atoms at shell sites. Using such building units, bulk metallic glasses (BMGs) can be formed. This strategy was verified in the Cu–Zr binary system, where the existence of $Cu_8Zr_5$ icosahedral clusters in $Cu_{61.8}Zr_{38.2}$, $Cu_{64}Zr_{36}$, and $Cu_{64.5}Zr_{35.5}$ amorphous alloys has been demonstrated. In other words, a lot of studies have been done to investigate the electronic structures and geometries of Cu-rich Cu–Zr clusters and Cu-based alloys, while there is still a lack of investigation of Zr-rich $Zr_nCu$ clusters.

Although a lot of studies have been done, it is still a challenge to determine the relationship between microstructure and properties because of the huge number of possible candidates[33] and the computational cost of DFT as $O(N^3)$.[34,35] In 2017, after a detailed investigation of the

†Corresponding author. E-mail: xjcxh0991@xju.edu.cn
‡Corresponding author. E-mail: dhm@xju.edu.cn

© 2024 Chinese Physical Society and IOP Publishing Ltd 

amorphous alloy material database and an analysis of the descriptor related to the glassy formation ability, Sun *et al.*[36] proposed that the machine-learning algorithm model could be used when designing amorphous alloys. In 2020, Tong *et al.*[37] successfully searched the $B_{84}$ cluster structure using the CALYPSO code combined with machine-learning potential (MLP). With the rapid development of artificial intelligence (AI), the use of machine learning has risen in different fields and has made significant progress. As one of the key tools in data-driven material research methods,[38,39] it has been widely used to calculate the physical and chemical properties[40–49] and screen out novel materials[50–55] due to its high computational efficiency and accuracy. Recently, various machine-learning models have been introduced to construct an accurate potential energy surface (PES) using the first principles data.[56,57] The obtained MLP[58–60] can be used to learn the mapping between structures and energy. In 1995, Blank *et al.*[61] first constructed a molecular potential energy surface using a neural network, and then various MLPs were proposed and developed.[62–67]

In order to investigate the electronic structures and geometries of Zr-rich Zr–Cu clusters, the authors calculated the geometry and electronic structures of $Zr_nCu$ ($n = 2$–12) clusters using both MLP and DFT. The stable and metastable geometries of $Zr_nCu$ ($n = 2$–12) clusters were obtained using the CALYPSO method combined with MLP in atom-centered symmetry functions (ACSF),[68,69] which is obtained from the first-principles data. The results obtained by MLP are similar to the DFT results while the MLP is two or three orders of magnitude faster than DFT. The electronic structures, growth pattern, magnetic moments, and chemical bonds are further investigated using DFT. The results show that the $Zr_nCu$ ($n \geq 3$) clusters possess three-dimensional geometries, $Zr_nCu$ ($n \geq 9$) possess cage-like geometries, and $Zr_{12}Cu$ has an icosahedral geometry. The binding energy per atom gradually became enlarged with the increase in the size of the clusters, and $Zr_nCu$ ($n = 5$, 7, 9, 12) have relatively stronger stability than their neighbors do. The magnetic moment of most $Zr_nCu$ clusters is just $1\mu_B$, and the main components of HOMOs come from the Zr-d state. There are hardly any localized two-center bonds, and there are about 20 $\sigma$-type delocalized three-center bonds.

## 2. Methods and applications

### 2.1. Machine-learning potentials in atomic-centered symmetry functions

The MLP of Zr–Cu binary metal clusters was first trained and tested using the first-principles data obtained by the spin-polarized DFT implemented in the VASP package.[70,71] In order to get accurate first-principles data, the calculation was performed using the following parameters. The Perdew–Burke–Ernzerhof (PBE)[72] functional based on the generalized gradient approximation (GGA)[73] was used to represent electronic exchange–correlation energy functions, and the cut-off energy was set as 295 eV.

The MLP adopted the ACSF descriptor.[37,74,75] The MLP was trained by gradually enlarging the size of the training set from 400–8000. Figure 1 illustrates the evolution of the root mean square error (RMSE) of the energy, force, and stress tested on the testing set. As shown in Fig. 1, the RMSE for energy, force, and stress was gradually reduced by increasing the size of the training set. Note that the obtained RMSE of energy, force, and stress are 0.024, 0.184, and 0.024 when the size of the training set is 8088. The MLP is accurate enough to predict stable candidates of Zr–Cu binary clusters.

The obtained MLP was used to predict the stable structures of the $Zr_nCu$ ($n = 2$–12) and $Zr_nCu_{13-n}$ ($n = 3$–10) clusters via the CALYPSO code. For comparison, the global lowest energy structures of $Zr_nCu$ ($n = 10$, 11) are also predicted via the CALYPSO code and VASP code, which are used to do local structure optimization. The results obtained from the former method (MLP) are similar to the latter, while the computational cost of the former is about 2–3 order of magnitude less than the latter. The obtained lowest-energy structures of the $Zr_nCu_{13-n}$ ($n = 3$–10) clusters using the MLP (shown in Fig. 2) are well consistent with the DFT results obtained by Jiang *et al.*[26]

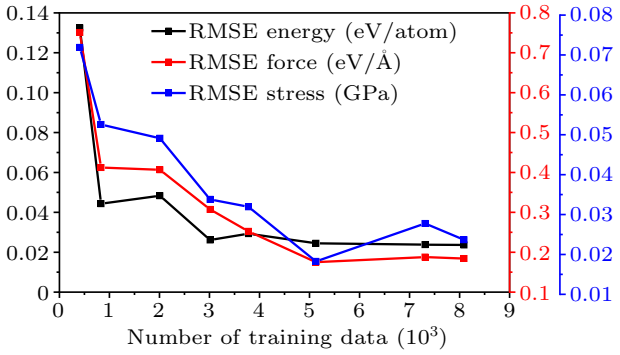



**Fig. 1.** The evolution of the RMSE for the energy (eV·atom$^{-1}$), force (eV·Å$^{-1}$), and stress (GPa) tested on different testing sets.

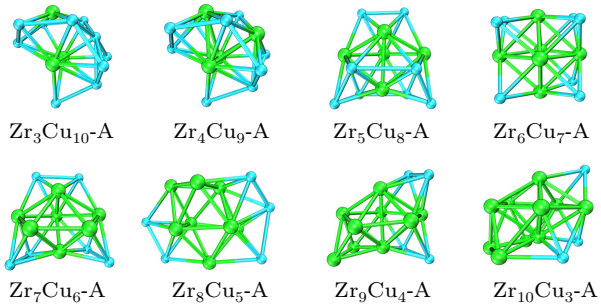



**Fig. 2.** Ground state structure of the $Zr_nCu_{13-n}$ ($n = 3$–10) clusters searched by MLP (green balls represent Zr atoms, cyan balls represent Cu atoms).

### 2.2. Application of MLP to predict the structures of the $Zr_nCu$ clusters

The stable structures of the $Zr_nCu$ ($n = 2$–12) clusters were further screened using CALYPSO[76–78] code and the obtained Zr–Cu MLP. CALYPSO is an efficient structural prediction method based on particle swarm optimization (PSO).[79] During the structure prediction simulation, about 100 generations along with 40 isomers per generation were chosen. Except for the first generation whose geometries were randomly generated, about 20% of the isomers of the other generation were inherited from the previous generation, and the rest were still randomly generated. After 100 generations of evolution, several candidates were obtained. Noting that some of these candidates may have similar geometry that should be merged using the structure prototype analysis package (SPAP).[80]

### 2.3. Physical properties of $Zr_nCu$ clusters

The screened candidates are further reoptimized using spin-polarization DFT. The spin-polarized electronic structures of the $Zr_nCu$ ($n = 2$–12) clusters were also investigated using the Gaussian09[81] code with B3LYP/def2TZVP. All calculations are carried out with ultrafine precision. The electronic local function (ELF) and adaptive natural density partitioning (AdNDP)[82] bonding analysis were calculated with the Multiwfn[83] software. VMD[84] software is used to visualize the clusters' MO (MO) and AdNDP.

## 3. Results and discussion

### 3.1. Stable geometries of $Zr_nCu$ ($n = 2$–12) clusters

Using the method described above, several stable geometries were obtained (shown in Fig. 3). Point group and relative energy comparison with the lowest energy of each of the clusters are also given in the comments in Fig. 3. For each structure, $n$A, $n$B, and $n$C represent the ground state, metastable and sub-metastable structures of the $Zr_nCu$ ($n = 2$–12) clusters, respectively. For the $Zr_2Cu$ cluster, 2A isomer is a one-dimensional structure of Cu atoms on the outer side. For the $Zr_3Cu$ cluster, 3A is the tetrahedral configuration with the highest symmetry. For the $Zr_4Cu$ cluster, the configuration of 4A is a trigonal bipyramid structure, and its geometric structure shows that a Zr atom is derived from the configuration of 3A. For the $Zr_5Cu$ cluster, the 5A configuration can be regarded as coming from the 4A configuration, which is formed by adding a Zr atom with a face cap. For the $Zr_6Cu$ cluster, 6A geometry is a pentagonal biconical structure with $C_s$ symmetry and can be considered to have been derived by adding a Zr atom to the 5A configuration. For the $Zr_7Cu$ cluster, the 7A

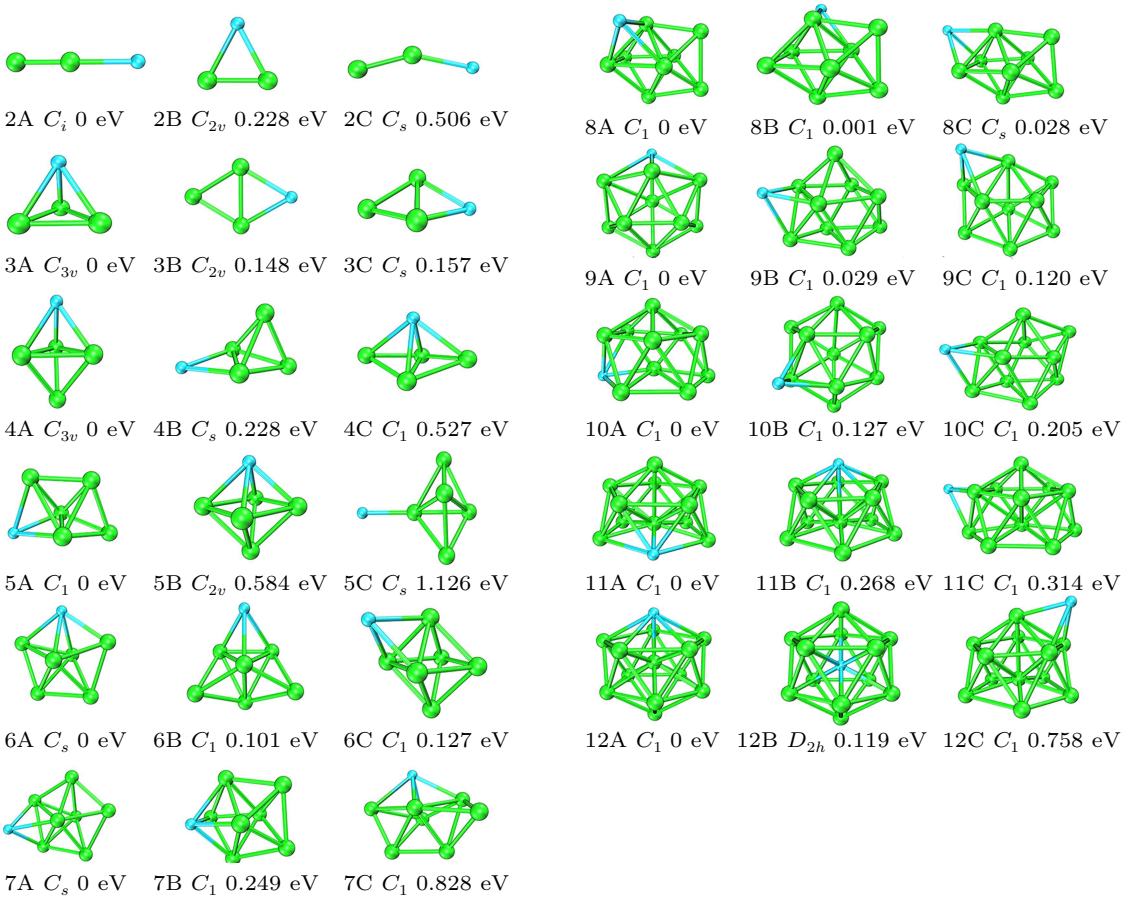



**Fig. 3.** The geometry of the three lowest energy isomers of the $Zr_nCu$ ($n = 2$–12) nanoclusters searched by MLP, and the energy difference in electronvolts from the lowest energy isomer at the same size (green balls represent Zr atoms, cyan balls represent Cu atoms).

configuration is composed of seven Zr atoms forming a pentagonal biconical structure and a Cu atom added to the outside. Unlike the 6A configuration, the Cu atoms no longer form a pentagonal biconical structure, but are transferred to the outside. For the $Zr_8Cu$ cluster, 8A has $C_1$ symmetry, and the geometric configurations of 8A, 8B, and 8C all show that an atom is added to the 7B configuration, and the Cu atom in the 7B configuration is transferred to a new position. The 8B configuration is a mirror of the operation of the 8A configuration, and the energy of the two is similar. 8C has $C_s$ symmetry, and the position of Cu in the 8C configuration is different from that of 8A and 8B. For the $Zr_9Cu$ cluster, 9A configuration is a cage-like structure of a hexadecahedron and the structural framework has also changed from a three-dimensional structure to a cage-like structure. For the $Zr_{10}Cu$ cluster, the 10A configuration is derived from the 9A configuration, and the symmetry is a $C_s$ octahedral cage structure. For the $Zr_{11}Cu$ cluster, 11A has $C_1$ symmetry, and it is derived from the 10A configuration with a Zr atom added inside; different from the 11A configuration, the Cu atoms in the 11B and 11C configurations are at the top and outside, respectively. For the $Zr_{12}Cu$ cluster, both the 12A and 12B configurations are icosahedrons, with Cu atoms on the outside and inside, respectively. It is worth mentioning that 12B is an icosahedron with $D_{2h}$ symmetry. In addition, further structural analysis is provided in the supplementary materials.

### 3.2. Relative stabilities

It is worth investigating the relative stabilities and the growth pattern because the magic clusters play an important role in determining the physical properties like glassy formation ability. Herein the relative stabilities and growth pattern are evaluated by binding energy per atom ($E_b$), second-order energy difference ($\Delta_2E$), fragmentation energy ($E_d$), and spin-polarized HOMO–LUMO gap, which are defined as the following equations:

$$E_b(Zr_nCu) = [nE(Zr) + E(Cu) - E(Zr_nCu)]/(n+1), \quad (1)$$

$$\Delta_2E = E(Zr_{n-1}Cu) + E(Zr_{n+1}Cu) - 2E(Zr_nCu), \quad (2)$$

$$E_d(Zr_nCu) = E(Zr_{n-1}Cu) + E(Zr) - E(Zr_nCu), \quad (3)$$

$$E_{gap} = E_{LUMO}(Zr_nCu) - E_{HOMO}(Zr_nCu), \quad (4)$$

where $E(Zr)$ and $E(Cu)$ respectively represent the energy of an isolated Zr atom and Cu atom. $E(Zr_nCu)$, $E(Zr_{n-1}Cu)$ and $E(Zr_{n+1}Cu)$ respectively, represent the total energy of the corresponding clusters. $E_{LUMO}(Zr_nCu)$ and $E_{HOMO}(Zr_nCu)$ represent the lowest unoccupied molecular orbital (LUMO) and the highest occupied molecular orbital (HOMO) energy, respectively.

The obtained values of binding energy per atom ($E_b$), second-order energy difference ($\Delta_2E$), fragmentation energy ($E_d$), and spin-polarized HOMO–LUMO gap are shown in Figs. 4(a)–4(c) and Table 1.

As shown in Fig. 4(a), the binding energy per atom ($E_b$) gradually became enlarged with increasing cluster size, implying the cage-like clusters are more stable than small-sized clusters. We found that icosahedron clusters have the highest stability, which may cause the widespread existence of icosahedron clusters in amorphous alloys. Meanwhile, as shown in Fig. 4(b), $Zr_nCu$ ($n$ = 5, 7, 9) may be more stable than their neighbor clusters due to the local peak of ($\Delta_2E$).

Similar to Fig. 4(a), the fragmentation energy (shown in Fig. 4(c)) also became enlarged with the increase in cluster size, and some peak can also be found when the cluster size is 5, 7, and 9, indicating these clusters may be more stable than their neighbor clusters.

**Table 1.** The symmetries, $E_b$ (eV), $\Delta_2E$ (eV), $E_d$ (eV), $\alpha$-$E_{gap}$ (eV), $\beta$-$E_{gap}$ (eV), Mag ($\mu_B$), and charge $Q$ ($e$) on Cu of the $Zr_nCu$ ($n$ = 2–12) clusters.

| Cluster | Sym. | $E_b$ | $\Delta_2E$ | $E_d$ | $\alpha$-$E_{gap}$ | $\beta$-$E_{gap}$ | Mag | $Q$ (Cu) |
|---|---|---|---|---|---|---|---|---|
| $Zr_2Cu$ | $C_s$ | 2.260 | | | 1.425 | 2.150 | 1 | −0.133 |
| $Zr_3Cu$ | $C_{3v}$ | 2.856 | −0.735 | 4.644 | 1.702 | 1.388 | 3 | −0.085 |
| $Zr_4Cu$ | $C_{3v}$ | 3.360 | −0.031 | 5.379 | 1.537 | 1.388 | 3 | −0.008 |
| $Zr_5Cu$ | $C_1$ | 3.702 | 0.177 | 5.410 | 1.463 | 1.366 | 1 | −0.148 |
| $Zr_6Cu$ | $C_s$ | 3.921 | −0.366 | 5.234 | 1.269 | 1.278 | 1 | −0.122 |
| $Zr_7Cu$ | $C_s$ | 4.131 | 0.598 | 5.600 | 1.141 | 1.316 | 1 | −0.255 |
| $Zr_8Cu$ | $C_1$ | 4.228 | −0.438 | 5.002 | 1.135 | 1.107 | 1 | −0.200 |
| $Zr_9Cu$ | $C_s$ | 4.349 | 0.067 | 5.440 | 1.017 | 1.208 | 1 | −0.211 |
| $Zr_{10}Cu$ | $C_s$ | 4.442 | −0.251 | 5.373 | 1.075 | 1.085 | 3 | −0.212 |
| $Zr_{11}Cu$ | $C_s$ | 4.541 | −0.692 | 5.624 | 1.122 | 1.066 | 1 | −0.277 |
| $Zr_{12}Cu$ | $C_s$ | 4.677 | | 6.316 | 1.025 | 1.255 | 1 | −0.723 |

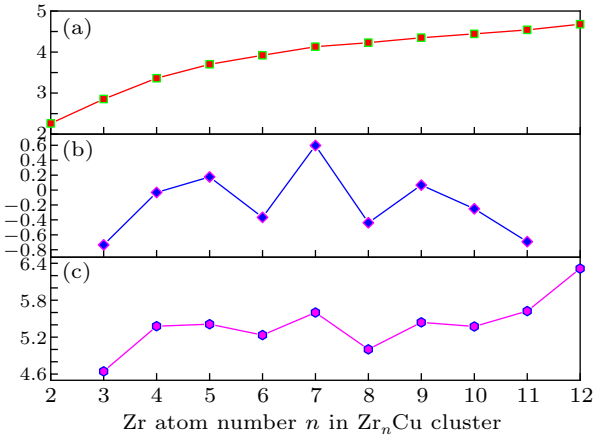



**Fig. 4.** Size dependence of (a) the averaged binding energy ($E_b$), (b) the second-order energy difference ($\Delta_2E$), and (c) the dissociation energy ($E_d$) for the lowest energy $Zr_nCu$ ($n$ = 2–12) clusters.

### 3.3. Magnetic moments and electronic structures

The magnetic moments of the $Zr_nCu$ ($n$ = 2–12) clusters are also obtained (shown in Table 1). As shown in Table 1, except for $Zr_nCu$ ($n$ = 3, 4, 10) whose magnetic moments are $3\mu_B$, the magnetic moments of other clusters are all $1\mu_B$. To better understand the electronic structures of these clusters, the atomic charges are firstly evaluated using the Mulliken

population analysis.[85] As shown in Table 1, the obtained atomic charge of Cu atom varied from −0.133 ($Zr_2Cu$) to −0.723 ($Zr_{12}Cu$), indicating electron transfer occurred among the Zr and Cu atoms and the Cu atom is an electron acceptor. It is not surprising that the Cu atom could be an electron acceptor because Cu atoms have relatively larger Pauli electronegativity (about 1.90) than the Zr atom (about 1.33).[86] The number of transferred electrons has a relation to the interaction between Cu and Zr atoms. For example, as shown in Fig. S3, $Zr_{12}Cu$ has the shortest neighboring Zr–Cu bond (2.58 Å), which makes it have the strongest bond energy per atom and the largest transferred electrons (−0.723).

The ELF is also obtained to analyze the electronic structures of $Zr_nCu$ ($n$ = 2–12) clusters. In order to simultaneously characterize the bonding regions of Zr–Zr and Zr–Cu in the ELF diagram, for each system, this paper selects a two-dimensional ELF plane determined by Cu atoms and two Zr atoms adjacent to Cu atoms, three atoms. Figures 5 and S2 show a two-dimensional diagram of the ELF value for the ground-state $Zr_nCu$ ($n$ = 2–12) clusters. Figure 5 shows the ELF value of the $Zr_nCu$ ($n$ = 5, 7, 9, 12) clusters. As shown in Fig. 5, the ELF in the region between the Zr and Cu atoms is about 0.35–0.50, indicating this region has a value like uniform electron gas.[87] The ELF in the region among Zr atoms is very close to zero, indicating the electrons among Zr atoms should be delocalized. That is to say the Zr–Zr chemical bond should be a metallic bond.

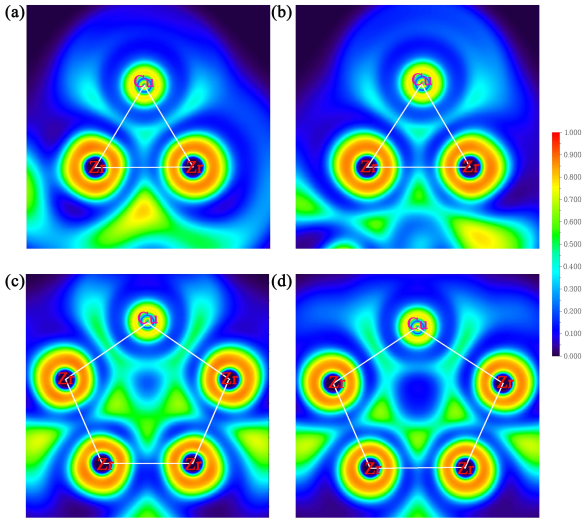



**Fig. 5.** The two-dimensional ELF of the (a) $Zr_5Cu$, (b) $Zr_7Cu$, (c) $Zr_9Cu$, and (d) $Zr_{12}Cu$ clusters.

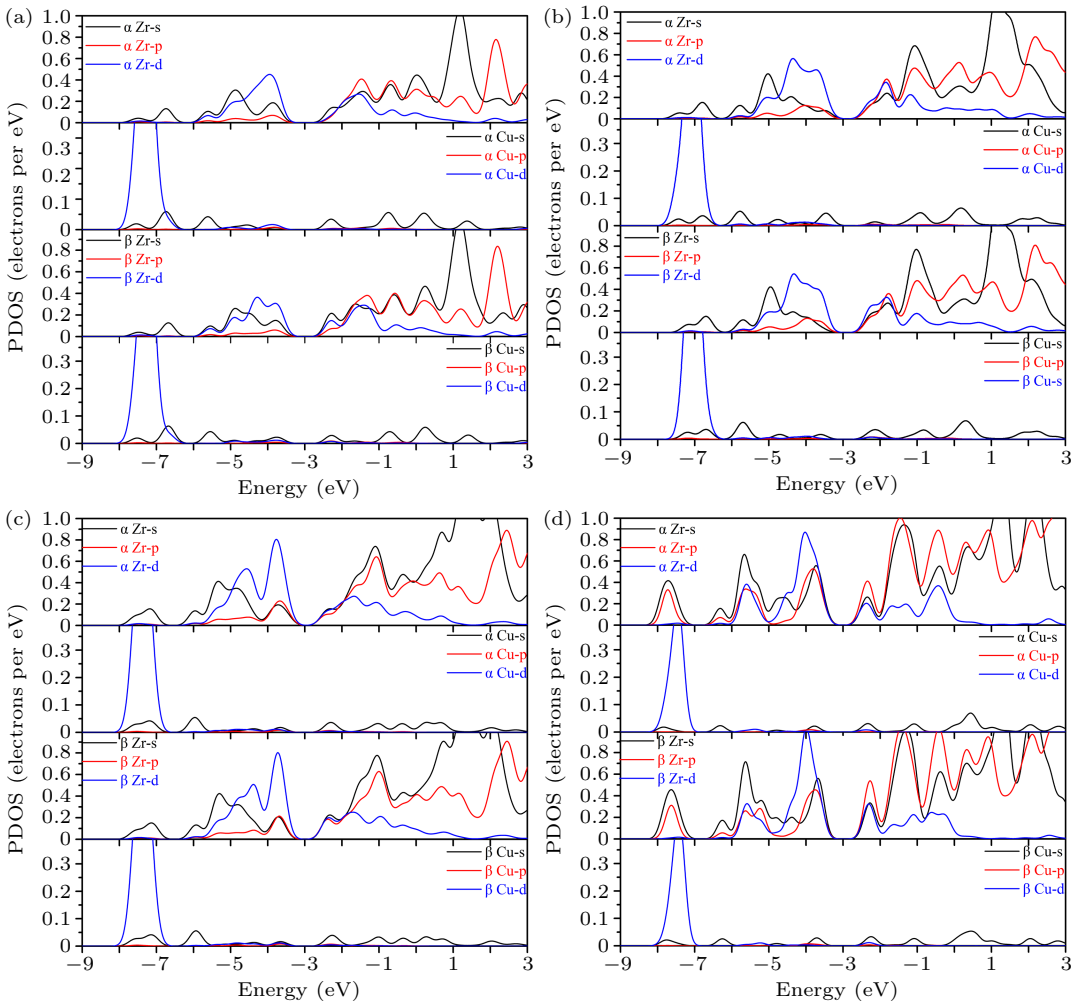



**Fig. 6.** The PDOS of the Cu and Zr atoms in (a) the lowest-energy $Zr_5Cu$ cluster, (b) the lowest-energy $Zr_7Cu$ cluster, (c) the lowest-energy $Zr_9Cu$ cluster, and (d) the lowest-energy $Zr_{12}Cu$ cluster.

The partial density of states (PDOS) and difference plot of the $Zr_nCu$ ($n = 5$, 7, 9, 12) clusters are also obtained, respectively (shown in Figs. S6 and S3). As shown in Fig. 6, on the one hand, the PDOS on the HOMO originates mainly from the 4d and 4s electrons of Zr. On the other hand, far away from the HOMO level region (approximately $-7.5$ to $-6.5$ eV), the main contribution is from the 3d electrons of Cu atoms as a universal rule in $Zr_nCu$ clusters.

### 3.4. MOs of the icosahedral cluster

As described by Wang *et al.*,[29] the icosahedral cluster plays an important role in determining the glassy formation ability, and the microstructure in the amorphous alloy may be the metastable cluster, hence hereafter the authors provide a detailed investigation into the MOs of a metastable $Zr_{12}Cu$ cluster (marked as 12B in Fig. 1). The obtained diagram of MOs and corresponding energy levels of the 12B cluster are shown in Fig. 3, and the s, p, and d components of spin-polarized MOs are shown in Table 2.

As shown in Fig. 7, 12B is an open shell cluster and the total magnetic moment is $1\mu_B$. The spin-polarized HOMO–LUMO gap of 12B is 0.934 eV (spin up) and 1.164 eV (spin down). As shown in Table 2, the Zr atoms, especially the Zr-d states and Zr-s states make the main contribution to the HOMO, and the MOs below HOMO, while the Cu-s, and Cu-p states hardly contribute to the total states. For example, about 47.80% and 62.15% of $\alpha$-HOMO and $\beta$-LUMO come from the Zr-d states.

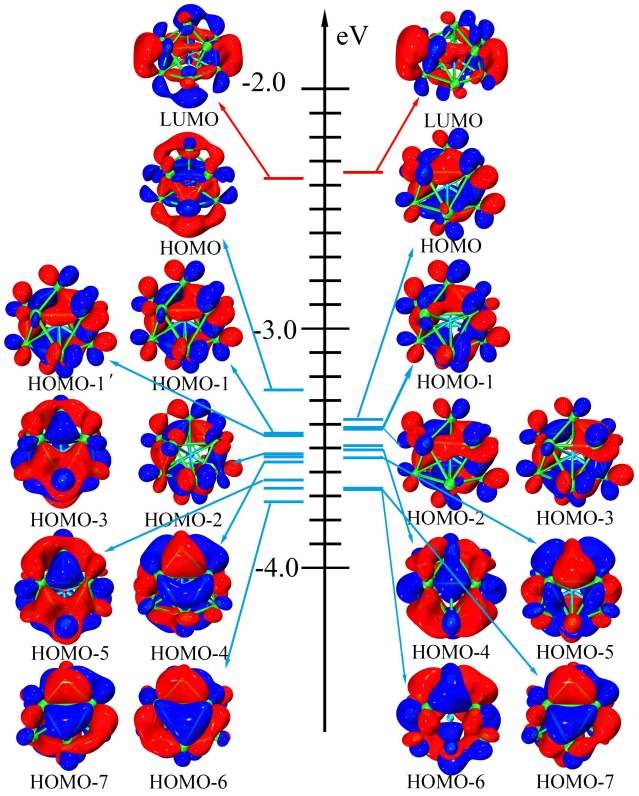



**Fig. 7.** MOs and corresponding energy levels of the 12B cluster.

**Table 2.** The s, p, and d components of the spin-polarized LUMO and serval HOMOs in the 12B cluster (– represents atomic orbital composition less than 0.5%).

| | $\alpha$ | | | | | | $\beta$ | | | | | |
|---|---|---|---|---|---|---|---|---|---|---|---|---|
| | Zr-s | Zr-p | Zr-d | Cu-s | Cu-p | Cu-d | Zr-s | Zr-p | Zr-d | Cu-s | Cu-p | Cu-d |
| LUMO | 27.05 | 20.92 | 45.32 | 1.07 | – | 5.60 | 25.51 | 18.40 | 43.73 | 5.09 | – | 7.25 |
| HOMO | 21.69 | 13.21 | 47.80 | 7.65 | – | 9.59 | 25.15 | 10.51 | 62.15 | – | – | 2.10 |
| HOMO-1 | 25.68 | 12.38 | 59.49 | – | – | 2.34 | 21.84 | 12.19 | 63.50 | 0.51 | – | 1.84 |
| HOMO-1′ | 26.55 | 11.32 | 60.28 | – | – | 1.76 | – | – | – | – | – | – |
| HOMO-2 | 25.46 | 10.48 | 62.40 | – | – | 1.57 | 14.18 | 10.50 | 73.63 | – | – | 1.59 |
| HOMO-3 | 1.41 | 15.85 | 82.53 | – | – | – | 15.11 | 10.11 | 73.51 | – | – | 1.17 |
| HOMO-4 | 9.19 | 15.15 | 75.47 | – | – | – | 14.53 | 15.55 | 69.75 | – | – | – |
| HOMO-5 | 21.48 | 10.17 | 67.54 | – | – | 0.71 | 7.65 | 15.30 | 76.85 | – | – | – |
| HOMO-6 | 11.75 | 12.55 | 75.53 | – | – | – | 19.67 | 13.42 | 66.18 | 0.58 | – | – |
| HOMO-7 | 8.45 | 13.32 | 78.04 | – | – | – | 9.26 | 13.68 | 76.88 | – | – | – |

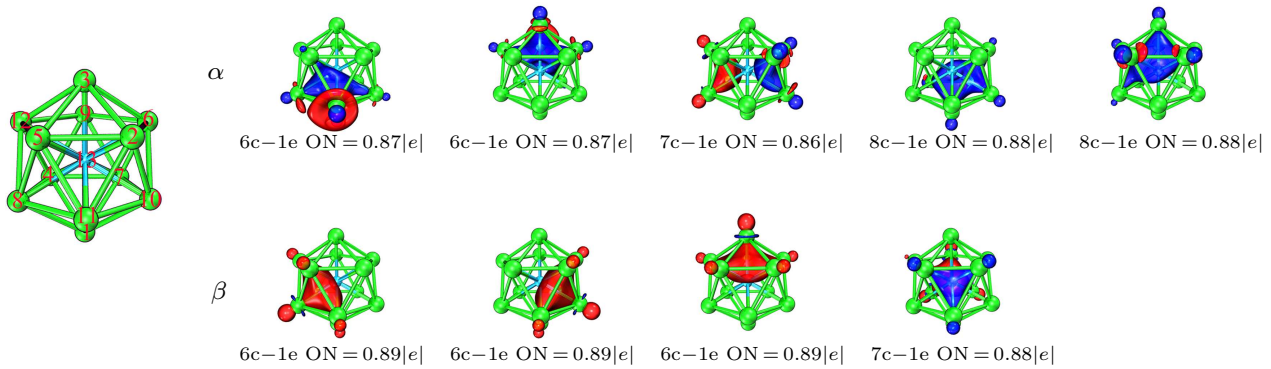



**Fig. 8.** The 6c–1e chemical bond analyzed by the AdNDP method. ON means the occupancy number.

The chemical bonds of the 12B cluster are further investigated using the AdNDP method.[82] After a detailed investigation of these chemical bonds, the authors found that there are five single-center single electron bonds in spin-up and spin-down states, respectively, while there is not one dual-center single electron bond (as shown in Fig. S3). The delocalized multi-center single electron bonds in each spin-polarized state are shown in Figs. 8 and S4. As shown in Fig. S4, there are 20 three-center single electron bonds in each spin-polarized state, and these three-center bonds should be $\sigma$ bonds. There were two 6c–1e $\sigma$-orbitals in spin-up states, each of which occupied 0.87 electrons. There is also one 7c–1e $\sigma$-orbital with an occupancy number (marked as ON) of 0.86$e$, and two 8c–1e $\sigma$-orbitals with an ON of 0.88$e$ in spin-up states. Unlike the spin-up state, there are three 6c–1e $\sigma$-orbitals with an ON of 0.89$e$ and one 7c–1e $\sigma$-orbital with an ON of 0.88$e$ in the spin-down states.

## 4. Conclusion and perspectives

In this paper, the low-energy isomers of $Zr_nCu$ ($n = 2$–12) clusters are screened out using the CALYPSO code and MLP. The MLP was trained and tested using the first-principles data of $Zr_nCu$ ($n = 2$–11) clusters. The obtained MLP is further used to screen out the low-energy candidates of $Zr_nCu$ ($n = 2$–12) clusters, and the results are similar to the results obtained by CALYPSO and DFT, but the MLP method can be faster by two or three orders of magnitude. The electronic structures, growth pattern, magnetic moments, and chemical bonds are further investigated using the DFT.

The results show that the $Zr_nCu$ ($n \geq 3$) clusters possess three-dimensional geometries, $Zr_nCu$ ($n \geq 9$) possess cage-like geometries, and $Zr_{12}Cu$ possesses icosahedral geometry. The binding energy per atom gradually became enlarged with the increase in the size of the clusters, and $Zr_nCu$ ($n = 5$, 7, 9, 12) have relatively stronger stability than their neighbors. The magnetic moment of most $Zr_nCu$ clusters is just $1\mu_B$, and the main components of HOMOs come from the Zr-d state. There are hardly any localized two-center bonds, and there are about 20 $\sigma$-type delocalized three-center bonds.

## Acknowledgment

Project supported by the National Natural Science Foundation of China (Grant Nos. 11864040, 11964037, and 11664038).

## References

[1] Inoue A and Shen B 2002 *Mater. Trans.* **43** 766
[2] Zhang T, Inoue A and Masumoto T 1991 *Mater. Trans. JIM* **32** 1005
[3] Inoue A, Kato A, Zhang T, Kim S G and Masumoto T 1991 *Mater. Trans. JIM* **32** 609
[4] Sha Z D, Xu B, Shen L, Zhang A H, Feng Y P and Li Y 2010 *J. Appl. Phys.* **107** 063508
[5] Schroers J and Johnson W L 2004 *Phys. Rev. Lett.* **93** 255506
[6] Lu Z P and Liu C T 2003 *Phys. Rev. Lett.* **91** 115505
[7] Inoue A 2000 *Acta Mater.* **48** 279
[8] Hirata A, Kang L J, Fujita T, Klumov B, Matsue K, Kotani M, Yavari A R and Chen M W 2013 *Science* **341** 376
[9] Sheng H W, Luo W K, Alamgir F M, Bai J M and Ma E 2006 *Nature* **439** 419
[10] Inoue A and Zhang T 1996 *Mater. Trans., JIM* **37** 185
[11] Zhang Y, Mattern N and Eckert J 2011 *J. Appl. Phys.* **110** 093506
[12] Mattern N, Jóvári P, Kaban I Gruner S, Elsner A, Kokotin V, Franz H, Beuneu B and Eckert J 2009 *J. Alloys Compd.* **485** 163
[13] Xu D, Lohwongwatana B, Duan G, Johnson W L and Garland C 2004 *Acta Mater.* **52** 2621
[14] Wang H, Hu T, Qin J Y and Zhang T 2012 *J. Appl. Phys.* **112** 073520
[15] Wang Y, Wang Q, Zhao J and Dong C 2010 *Scr. Mater.* **63** 178
[16] Xia L, Li W H, Fang S S, Wei B C and Dong Y D 2006 *J. Appl. Phys.* **99** 026103
[17] Cheng Y Q, Ma E and Sheng H W 2009 *Phys. Rev. Lett.* **102** 245501
[18] Hui X, Fang H Z, Chen G L, Shang S L, Wang Y, Qin J Y and Liu Z K 2009 *Acta Mater.* **57** 376
[19] Mendelev M I, Sun Y, Zhang F, Wang C Z and Ho K M 2019 *J. Chem. Phys.* **151** 214502
[20] Sun Y L and Shen J 2009 *J. Non-Cryst.* **355** 1557
[21] Wen D D, Peng P, Jiang Y Q, Tian Z A, Liu R S and Dong K J 2014 *J. Non-Cryst. Solids* **388** 75
[22] Fujita T, Konno K, Zhang W, Kumar V, Matsuura M, Inoue A, Sakurai T and Chen M W 2009 *Phys. Rev. Lett.* **103** 075502
[23] Li M Z, Wang C Z, Hao S G, Kramer M J and Ho K M 2009 *Phys. Rev. B* **80** 184201
[24] Liu A C Y, Neish M J, Stokol G, Buckley G A, Smillie L A, de Jonge M D, Ott R T, Kramer M J and Bourgeois L 2013 *Phys. Rev. Lett.* **110** 205505
[25] Zhang Y, Mattern N and Eckert J 2012 *J. Appl. Phys.* **111** 053520
[26] Jiang Y Q, Lv J, He W X and Peng P 2021 *J. Mol. Liq.* **343** 117603
[27] Megha, Mondal K, Ghanty T K and Banerjee A 2021 *J. Phys. Chem. A* **125** 2558
[28] Trivedi R and Mishra V 2021 *J. Mol. Struct.* **1226** 129371
[29] Wang D, Zhao S J and Liu L M 2015 *J. Phys. Chem. A* **119** 806
[30] Sha Z D, Pan H, Pei Q X and Zhang Y W 2012 *Intermetallics* **26** 8
[31] Lekka C E 2010 *J. Alloys Compd.* **504** 190
[32] Yang L, Xia J H, Wang Q, Dong C, Chen L Y, Ou X, Liu J F, Jiang J Z, Klementiev K, Saksl K, Franz H, Schneider J R and Gerward L 2006 *Appl. Phys. Lett.* **88** 241913
[33] Stillinger F H and Weber T A 1982 *Phys. Rev. A* **25** 978
[34] Cogollo-Olivo B H, Seriani N and Montoya J A 2015 *Chem. Phys.* **461** 20
[35] Calaminici P, Pérez-Romero M, Vásquez-Pérez J M and Köster A M 2013 *Comput. Theor. Chem.* **1021** 41
[36] Sun Y T, Bai H Y, Li M Z and Wang W H 2017 *J. Phys. Chem. Lett.* **8** 3434
[37] Tong Q C, Gao P Y, Liu H Y, Xie Y, Lv J, Wang Y C and Zhao J J 2020 *J. Phys. Chem. Lett.* **11** 8710
[38] Schleder G R, Padilha A C M, Acosta C M, Costa M and Fazzio A 2019 *J. Phys. Mater.* **2** 032001
[39] Schmidt J, Marques M R G, Botti S and Marques M A L 2019 *npj Comput. Mater.* **5**
[40] Carrete J, Li W, Mingo N, Wang S D and Curtarolo S 2014 *Phys. Rev. X* **4** 011019
[41] Furmanchuk A o, Agrawal A and Choudhary A 2016 *RSC Adv.* **6** 95246
[42] Gaultois M W, Oliynyk A O, Mar A, Sparks T D, Mulholland G J and Meredig B 2016 *APL Mater.* **4** 053213
[43] Kim C, Pilania G and Ramprasad R 2016 *J. Phys. Chem. C* **120** 14575
[44] Kim C, Pilania G and Ramprasad R 2016 *Chem. Mater.* **28** 1304
[45] Isayev O, Oses C, Toher C, Gossett E, Curtarolo S and Tropsha A 2017 *Nat. Commun.* **8** 15679
[46] Yuan F and Mueller T 2017 *Sci. Rep.* **7** 17594
[47] Kauwe S K, Graser J, Vazquez A, and Sparks T D 2018 *Integrat. Mater. Manuf. Innovation* **7** 43
[48] Sosso G C, Deringer V L, Elliott S R and Csányi G 2018 *Mol. Simul.* **44** 866
[49] Zheng X L, Zheng P and Zhang R Z 2018 *Chem. Sci.* **9** 8426

[50] Oliynyk A O, Adutwum L A, Harynuk J J and Mar A 2016 *Chem. Mater.* **28** 6672
[51] Ward L, Liu R Q, Krishna A, Hegde V I, Agrawal A, Choudhary A and Wolverton C 2017 *Phys. Rev. B* **96** 024104
[52] Balachandran P V, Kowalski B, Sehirlioglu A and Lookman T 2018 *Nat. Commun.* **9** 1668
[53] Graser J, Kauwe S K and Sparks T D 2018 *Chem. Mater.* **30** 3601
[54] Li W, Jacobs R and Morgan D 2018 *Comput. Mater. Sci.* **150** 454
[55] Ryan K, Lengyel J and Shatruk M 2018 *J. Am. Chem. Soc.* **140** 10158
[56] Manzhos S, Dawes R and Carrington T 2015 *Int. J. Quantum Chem.* **115** 1012
[57] Jiang B, Li J and Guo H 2016 *Int. Rev. Phys. Chem.* **35** 479
[58] Behler J 2016 *J. Chem. Phys.* **145** 170901
[59] Mueller T, Hernandez A and Wang C 2020 *J. Chem. Phys.* **152** 050902
[60] Zuo Y X, Chen C, Li X G, Deng Z, Chen Y M, Behler J, Csányi G, Shapeev A V, Thompson A P, Wood M A and Ong S P 2020 *J. Phys. Chem. A* **124** 731
[61] Behler J and Parrinello M 2007 *Phys. Rev. Lett.* **98** 146401
[62] Schütt K T, Arbabzadah F, Chmiela S, Müller K R and Tkatchenko A 2017 *Nat. Commun.* **8** 13890
[63] Schütt K T, Sauceda H E, Kindermans P J, Tkatchenko A and Müller K R 2018 *J. Chem. Phys.* **148** 241722
[64] Shapeev A V 2016 *Multiscale Model. Simul.* **14** 1153
[65] Thompson A P, Swiler L P, Trott C R, Foiles S M and Tucker G J 2015 *J. Comput. Phys.* **285** 316
[66] Unke O T and Meuwly M 2019 *J. Chem. Theory Comput.* **15** 3678
[67] Bartók P, Payne M C, Kondor R and Csányi G 2010 *Phys. Rev. Lett.* **104** 136403
[68] Behler J 2011 *J. Chem. Phys.* **134** 074106
[69] Gastegger M, Schwiedrzik L, Bitterman M, Berzsenyi F and Marquetand P 2018 *J. Chem. Phys.* **148** 241709
[70] Kresse G and Furthmüller J 1996 *Comput. Mater. Sci.* **6** 15
[71] Wang V, Xu N, Liu J C, Tang G and Geng W T 2021 *Comput. Phys. Commun.* **267** 108033
[72] Ernzerhof M and Scuseria G E 1999 *J. Chem. Phys.* **110** 5029
[73] Perdew J P, Burke K and Ernzerhof M 1996 *Phys. Rev. Lett.* **77** 3865
[74] Tong Q C, Luo X S, Adeleke A A, Gao P Y, Xie Y, Liu H Y, Li Q, Wang Y C, Lv J, Yao Y S and Ma Y M 2021 *Phys. Rev. B* **103** 054107
[75] Tong Q C, Xue L T, Lv J, Wang Y C and Ma Y M 2018 *Faraday Discuss.* **211** 31
[76] Lv J, Wang Y C, Zhu L and Ma Y M 2012 *J. Chem. Phys.* **137** 084104
[77] Wang Y C, Lv J, Zhu L and Ma Y M 2010 *Phys. Rev. B* **82** 094116
[78] Wang Y C, Lv J, Zhu L and Ma Y M 2012 *Comput. Phys. Commun.* **183** 2063
[79] Eberhart R and Kennedy J 1995 *Proc. 6th Int. Symp. on Micro Machine and Human Science* 39
[80] Su C X, Lv J, Li Q, Wang H, Zhang L J, Wang Y C and Ma Y M 2017 *J. Phys.: Condens. Matter* **29** 165901
[81] Frisch M, Trucks G, Schlegel H, Scuseria G, Robb M, Cheeseman J, Scalmani G, Barone V, Mennucci B and Petersson G 2009 *Gaussian 09* (Revision C.01)
[82] Zubarev Y and Boldyrev A I 2008 *Phys. Chem. Chem. Phys.* **10** 5207
[83] Lu T and Chen F W 2012 *J. Comput. Chem.* **33** 580
[84] Humphrey W, Dalke A and Schulten K 1996 *J. Mol. Graph.* **14** 33
[85] Mulliken R S 1995 *J. Chem. Phys.* **23** 1833
[86] Pauling L 1932 *J. Amer. Chem. Soc.* **54** 3570
[87] Kohout M, Wagner F R and Grin Y 2002 *Theor. Chem. Acc.* **108** 150